PRV

PATENT- OCH REGISTRERINGSVERKET
Patentavdelningen

PCT / SE 2004 / 0 0 0 3 6 8

Intyg
Certificate

Härmed intygas att bifogade kopior överensstämmer med de handlingar som ursprungligen ingivits till Patent- och registreringsverket i nedannämnda ansökan.

This is to certify that the annexed is a true copy of the documents as originally filed with the Patent- and Registration Office in connection with the following patent application.

(71) *Sökande*   *Optillion AB, Stockholm SE*
    Applicant (s)

(21) *Patentansökningsnummer*   *0300774-7*
    Patent application number

(86) *Ingivningsdatum*   *2003-03-21*
    Date of filing

Stockholm, 2004-03-16

För Patent- och registreringsverket
For the Patent- and Registration Office

Marita Öun

Avgift
Fee   170:-

PRIORITY DOCUMENT
SUBMITTED OR TRANSMITTED IN
COMPLIANCE WITH
RULE 17.1(a) OR (b)

Acronyms

AC	Alternating Current
BR	Bit-Rate
BW	Bandwidth
cs	compressive (strain)
DC	Direct Current
FOM	Figure of Merit
EA	Electroabsorption
EAM	Electroabsorption Modulator
EO	Electro-Optic
ER	Extinction Ratio
FK	Franz-Keldysh
FM	Frequency Modulation
FQ	Frequency
HF	High Frequency
MZI	Mach-Zender Interferometer
MQW	Multi Quantum Well
OTDM	Optical Time Domain Multiplexing
PD	Photodiode
QCSE	Quantum Confined Stark Effect
QW	Quantum Well
SI	Semi-Insulating
SC	Semi Conductor
TDM	Time Domain Multiplexing
TML	Transmission Line
ts	tensile (strain)
TW	Traveling Wave

1. Introduction

1.1.

1.2. Recent progress in external optical modulators

There are generally two types of light intensity optical modulators, electro-optic (EO) and electroabsorption modulators (EAM). The EO modulator is based on interferometry where the refractive index is controlled by applying an external electrical field, usually implemented in form of a Mach-Zender Interferometer (MZI) []. Electroabsorption modulators are usually based on band to band absorption controlled by an external electrical field through the Frans-Keldych or quantum confined stark effect (QCSE). Resent material technologies have also enabled intra-band (inter sub-band) absorption close to the telecommunication wavelength of 1.55μm [].

The usual figure of merit (FOM) used for optical modulators [17][18][20] includes weighting of device parameters as drive voltage (V_{drive}), electrical bandwidth (3dBe), and DC load impedance (Z_L):

$$FOM = \frac{2 * Z_L}{50 + Z_L} f_{3dBe} \frac{\lambda}{1.55\mu m} V_{drive}$$

Where V_{drive} is the required voltage for a specified extinction ratio, e.g. 10dB [4], or 20dB [18] for electroabsorption modulators, and V_π for electrooptic modulators [17]. The required ER should reflect the application the device is intended to be used in, for example the current standards specifies 3dB for 10Gbit Ethernet (ieee 802.3) or slightly less than 10dB for SONET. *Higher extinction required for solitons...?*

Electroabsorption modulators usually have a strong interaction between the electrical and optical field and is therefore normally compact in size and show a low drive voltage. Therefore, the suggested FOM show a clear advantage in favour for EAMs [18] [4]. The compatible process for integration together with a laser, as well as the possibility to design with low polarization sensitivity can further motivate the use of an EAM. The electrooptic modulator does however show other advantages not included in this FOM such as well-defined non-linearity and controllable chirp. [ref]

A summary of reported EAM devices with an electrical bandwidth more than 30GHz is presented in Table 1.

Group	dBe	Length [μm]	10dB ER [V]	Comment
InGaAs/InAlAs:				
Tamura, NTT 2003 [2]	-2dB @ 50GHz	75	0.85	InGaAlAs / InAlAs
Ido, Hitachi 1996 [3]	-3dB @ 50GHz	63	0.95	
Devaux, CNET 1995 [4]	-3dB @ 42GHz	75	0.75	
Moodie, Corning 2001 [5]	-3dB @ 34GHz	?	2	chirp<1
InGaAsP/InGaAsP:				
Mineo, Oki 2001 [6]	-2.5dB@50GHz	100	0.65	
Fu, Red Clover NW 2002 [7]	-2dB @ 50GHz	?	1.3	
Feng, Fujitsu 2002 [8]	±0dB @ 50GHz	70	dynamic 9dB 3.9V	LCL tuned
Tada, Mitsubishi 2002 [9]	-3dB @ 45GHz	75	1.2	
Miyazaki, Mitsubishi 2002 [10]	-3dB @ 30GHz	?	dynamic 11dB 2.4V	chirp < 1 asymmetric QW
Takagi, Mitsubishi 2001 [11]	-3dB @ 35GHz	75	1.4	chirp <1
Mason, Agere / Lucent 2002 [12]	-3dB @ 38 GHz	120	0.9	Tandem
	-2dB @ 50 GHz	80	?	
TML-EAM InGaAsP/InGaAsP:				
Shirai, Hitachi / OpNext 2002 [13]	-3dB @ 35GHz	150	24dB @ 2.5V	ICB $Z_L=50\Omega$
Chiu, UCSB 2002 [14]	-1.5dB @ 20GHz	300	0.35	$Z_L=35\Omega$
Akage, NTT 2001 [15]	-2dB @ 50GHz	225	0.9	$Z_L=50\Omega$
Li, UCSD 2001 [16]	-3dB @ 35GHz	200	slope eff. 0.65V^{-1}	$Z_L=26.2\Omega$, $\lambda=1.3\mu m$, bulk
Our work 1st gen., KTH 2001	-2dB @ 50GHz	450	0.6	$Z_L=13\Omega$ bulk
Our work 2nd gen., KTH/Optillion 2003	±0dB @ 50GHz	2*100	2.2	$Z_L=35\Omega$

Table 1. Reported electroabsorption modulator with an electrical bandwidth over 30GHz. The specified values are often extracted graphically from figures and should be considered as quantitative.

Recently, modulators designed for 40Gbit transmission links have matured and several groups have reported a 3dBe bandwidth exceeding 50GHz. To the best of my knowledge there is so far no reported measurements on EAMs beyond this frequency. This frequency limit is often related to the limitation of the Agilent lightwave component analyser 86030A. Either the devices have been characterized with this analyser, or the measurements are related to this device for calibration reasons. For example, as in our case, the photodetector is calibrated with this analyser (chapter **Error! Reference source not found.**). Measurements on optical modulators at higher frequencies up to 110GHz have only been reported for Ti:LiNbO₃ [21] and polymer [22], [23] EO modulators. This LiNbO₃ modulator showed a 3dBe bandwidth of 70 GHz with a

V_x of 5.1V, this is the highest *verified* bandwidth reported to this date. The polymer modulator only presents optical FM response in separated bands, there is no reports on the corresponding broadband response from DC to 110GHz. The same group has also presented a MZI intensity modulator; the frequency response was however not presented due to high electrode attenuation [24].

Due to the common trend of only reporting the optical response up to 50GHz it is difficult to quantitatively compare the different devices with respect to the conventional FOM (ref) at this time. Some groups reports of extrapolated 3dBe bandwidths, for example: NTT [15] 70GHz, UCSB [14] 40GHz, and our second generation modulator indicates a BW of slightly more than 90GHz (chapter 4). Especially TML-EAMs show different type of transfer functions depending · on the dominating BW limitation (chapter 3.3), therefore a reliable extrapolation requires a complete set of TML parameters and comprehensive modeling. (TA bort/Ändra)

1.3. Basic Operation of Electro-Optical Converters

EAMs and p-i-n photodetector are based on photon absorption arising from band-to-band excitation of an electron hole pair in a depleted intrinsic region. In a p-i-n photodetector the band-gap is lower than the photon energy, for the telecom wavelength of 1.55μm or 1.3μm the usual absorption layer material is InGaAs (E_g=0.75eV). In EAMs the bandgap is slightly higher than the photon energy, and the absorption utilizes the Franz-Keldysh (FK) effect [17] (Fig. 1). Here the probability of absorption increases due to the perturbation of the wave function with an external applied filed. A simple way to explain this effect is to say that the electron is excited to a virtual state close to the bandgap, the probability of absorption is then proportional to the tunnel probability between this virtual excited state and the conduction band (Fig. 1). The barrier thickness is decreased with a strong applied external electrical field, and the absorption probability is increased.
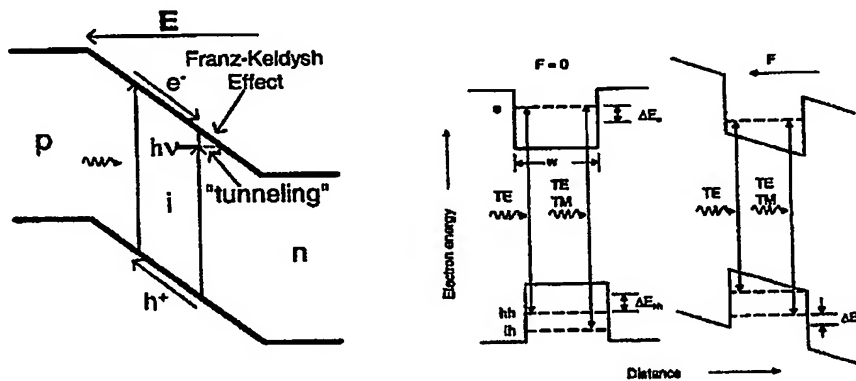
Fig. 1. Principe of light absorption and photocurrent generation in a EAM and p-i-n Photodetector. Left figure illustrates bulk band-to-band absorption and the Franz-Keldysh effect, the right figure (from [19]) illustrates the quantum confined Stark effect (QCSE).

Utilizing the quantum-confined Stark-effect (QCSE) [] can enhance the electroabsorption effect. Also QCSE is based on the wave-function change that follows from an external field (Fig. 1). The QW absorption is enhanced by the exciton absorption present at room temperature [], as an effect the absorption has a very sharp peak for energy levels slightly below the band to band energy difference. This sharp exciton absorption enables a strong absorption shift with relatively small changes of the applied electrical field, the disadvantage is that QCSE devices is more wavelength sensitive than bulk FK devices.

Another disadvantage with QW devices is the escape time for excited carriers to leave the well; this slows the device down the when operated with high incoming optical power. This is specifically a problem for the hole transport due to the higher effective mass than the electron. The InGaAs/InAlAs material system show a larger band offset (deeper well) for the electrons than holes and is therefore an attractive solution for this reason (Table 1), however this material system requires MBE growth, and the process for straight mesa walls is more complicated than for the InGaAsP system [19].

Unstrained InGaAsP/InGaAsP wells show a larger band-offset for holes than electrons and is therefore disadvantageous with respect to high power saturation, this can however be improved by introducing strain compensated MQW devices. The choice of compressive (cs) or tensile (ts) strain in well and barrier respectively is important for the device properties. By using cs strain in the well and ts strain in the barrier the valence band offset for heavy holes (hh) is very much reduced, the offset for light holes (lh) can be designed to almost zero. This enables an effective hole transport which significantly improves the device performance under high power operation [25]. The disadvantage with this implementation is that only heavy holes contribute to the QCSE process, and the device can only be operated in the TE polarization (Fig. 1). Due to the high power capability this implementation is attractive when the device is integrated with a laser where the polarization state of the incoming light is controlled.

A more common implementation is to use ts strain in the wells and cs strain in the barriers. Tensile strain lifts the lh-band edge relative to the hh-band edge and the device can be designed to be polarization insensitive. In this design the lh- and hh-band becomes degenerated which causes a substantial deformation of the valence sub-bands [26]. As a result the effective mass model with the assumption of parabolic bands can no longer be applied. Devices with ts strained wells often show a pronounced exciton peak with a strong electroabsorption effect. Indeed most devices in Table 1 (when specified) utilize this design, resulting in very low drive voltages and high optical extinction.

Tensile strained QW devices show higher valence band offsets than cs strained QWs. The saturation improvement is therefore not so intuitive as for cs strained QW devices. The main argument is that the effectively reduced hole-mass in the well reduces the carrier escape time compared to unstrained material [19], input optical power levels up to 14dBm has been demonstrated without a significant penalty on the EA efficiency [14] (the polarization state of the incoming light is not specified).

2. Reactive Tuning and Traveling-Wave Structures

Electro-optic (EO) converters in general, and here specifically treated; p-i-n photodiodes (PD) and electro-absorption modulators (EAM) are often bandwidth limited by the junction capacitance (Fig. 1). This capacitive limitation can often be compensated by various implementations of passive reactive networks. In this chapter the basic concepts and implementations of reactive tuning will be introduced. Chapter 3 treats EAMs operating in the traveling-wave (TW) regime, in chapter 4 this concept is extended to segmented devices and TW-EAM structures, and chapter 5 is devoted to reactive p-i-n diode tuning.

2.1. Broadband Reactive Tuning

The method of compensating the capacitive load of an optical intensity modulator can be divided into three regimes (Fig. 2): lumped tuning, segmented transmission line (TML) tuning treated in chapter 4, and operation in the TW regime treated in chapter 3.
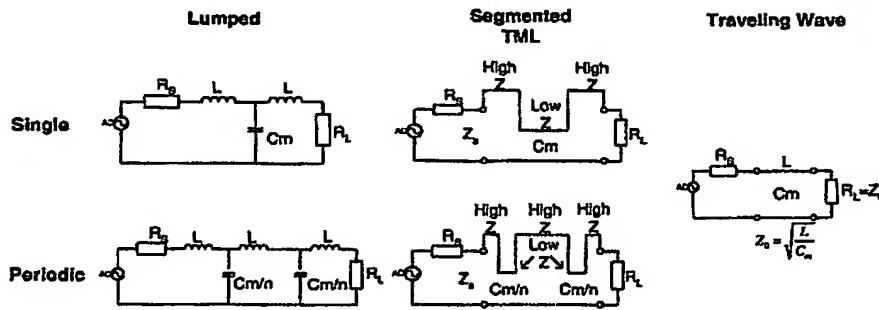

Fig. 2. Example of three different choices of implementations

The boundary between each regime can be related to the length scale of the layout implementation. Considering the transformed input impedance of a short TML with characteristic impedance Z_0 and propagation factor β terminated with the load Z_L:

$$Z_{in} = Z_0 \frac{Z_L + jZ_0 \tan(\beta l)}{Z_0 + jZ_L \tan(\beta l)} \approx \left\{ l \ll \lambda, \begin{matrix} Z_L < Z_0 \\ Z_L > Z_0 \end{matrix} \right\} \approx \frac{Z_L + j\omega L l}{\dfrac{Z_L}{1 + j\omega C l Z_L}} \qquad (2.1)$$

Where L and C is the equivalent capacitance and inductance per unit length of the TML, respectively. Thus a short section of a TML ($l \ll \lambda$) is well approximated as either a capacitance or inductance depending on the TML load compared to the characteristic impedance. (Walker [27] has investigated the difference between an ideal lumped modulator to a center fed and end fed TML with open termination, respectively). In fact, a short section of a high-impedance TML is a simple practical implementation of the matching inductor. The difference between the lumped and segmented TML regime can therefore be distinguished as the limit when distributed effects no longer can be neglected ($l \approx \lambda/8$). However, the segmented TML implementation also has an upper length limit when the segment length is close $l \approx \lambda/4$ the arising resonance degrades the performance of the device (see section 4.2).

The traveling wave (TW) regime is, in contrast to a standing wave, ideally distinguished as the case when the wave travels in only in one direction and is terminated in the load ($R_L = Z_0$). The length of a TW device can ideally be several wavelengths long, however, there is to the best of my knowledge so far no reports on a electro-absorption modulator (EAM) with a 3dB bandwidth larger than $l = 0.4*\lambda$ (see chapter 3). Also the periodic segmented TML can be operated as a TW device (although each modulator section is often well approximated as lumped modulators), this is further investigated in section 4.2.

Unfortunately, the terminology in the literature is often quite confusing, for example the single segmented TML is often (incorrectly) referred to as a TW modulator, even if it is clear that there is a significant termination mismatch ($R_L \neq Z_0$), i.e., the modulator is not operated in the TW regime. A more correct name including both segmented TML modulators and conventional (matched and not matched) TW modulators are, in my opinion, *distributed modulators* or *TML modulators*. An alternative name for a single segmented TML modulator has also been presented under the designation "impedance controlled electrode (ICE) modulator" [13].

2.2. Lumped LC-tuning (byt plats med föregående???)

Ideally the junction capacitance of an EAM or p-i-n diode can be compensated at a single frequency by a parallel inductance. The frequency limitation of this type of tuning is essentially limited by the loss dissipation, i.e., the Q value of the resulting resonance circuit. For wide-band operation this type of tuning is not feasible as the device is short circuited at low frequencies. The available approaches for baseband (DC to GHz range) are essentially more limited. The only allowed toolbox for lumped tuning consists of serial inductive tuning and parallel capacitive tuning (fig).

a) Lumped EAM tuning

FIGUR Example of lumped EAM tuning and corresponding transferfunction.

Using a lumped LC tuning for an EAM the transfer function is given as:

An inductance value of particular interest is L=XXX, where the filter correspond to the second order Bessel filter. Bessel filters are characterized by almost constant group delay across the entire passband, thus preserving the wave shape of filtered signals in the passband. At this point the BW is increased up to 35% compared to the corresponding RC limit. Increasing the inductance further does not increase the bandwidth but the transfer function is flattened and the return loss (S_{11}) is slightly decreased (at the expense of phase linearity). Serial inductive tuning in form of bond wire or flip-chip inductance is a natural implementation for device packaging. However, a typical problem is here that the inductance becomes too high, which can be compensated by an additional capacitor. Generally, adding even more elements to the LCLC chain adds the order of the filter and the ability to shape the transfer function to a desired goal function, however it also increases the required tolerance on each circuit components thus long filter chains without buffer amplifiers should be avoided except for very reproducible processes.

Lumped LCL tuning is widely used for device packaging and has been demonstrated to be feasible for EAMs operating up to the 40Gbit/s device generation [ref]. For higher frequencies it

is attractive to divide the device into several segments or to match the TML characteristic impedance to the matching resistor in a TW configuration. These implementations will be analyzed in detail in the following two chapters.

The p-i-n diode BW is limited by two conflicting effects; the RC time constant for thin intrinsic layer, and the transit time-effect associated with the carrier transport for thick intrinsic layers [ref]. Similar as for the EAM, the p-i-n diode the BW can be increased approximately 35% for a capacitance limited device. However a perhaps even more useful feature is the ability to compensate for the resulting transit time-delay that arises with a thick intrinsic layer. This is particularly useful when optimizing the responsivity of a vertical photodiode (VPD). This additional degree of freedom makes the inductive tuning for a p-i-n diode more complicated than for the EAM. paper XXX addresses the technical problem of increasing the BW with inductive tuning (or equalizing), while paper XXX discusses this issue from a fundamental perspective with respect to signal-to-noise ratio (SNR) optimization for VPDs. The results of these studies will be further discussed in chapter 5.

3. Design and Modeling of Electro-Absorption Modulators

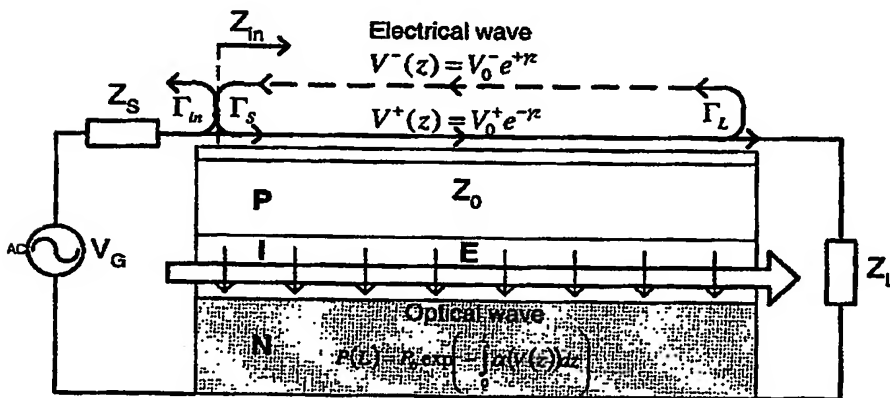### 3.1. Introduction to Traveling-Wave Electro-Absorption Modulators

Fig. 3. Principe of operation for a Traveling wave electro-absorption modulator (TWEAM)

Traveling-wave electro-absorption modulators (TWEAM) have proven to be an efficient solution in overcoming the capacitance limitation associated with a lumped configuration. Here the transmission line (TML) capacitance (dominated by the active junction capacitance) is compensated by the electrode inductance. The traveling wave (TW) implementation was successfully introduced for electro-optic (EO) modulators, and is now the dominating

implementation type for high-speed performance devices. TW devices have been demonstrated in several material systems including LiNbO$_3$ In the traveling-wave (TW) regime an electrical wave ideally co-propagates with the optical wave in the same direction and speed (Fig. 3). In a practical implementation ... For example in **paper xxx** we have demonstrated a 43GHz small signal bandwidth for 500μm long modulator with a TML capacitance of 1300pF/m terminated with a load resistance of 13Ω. The corresponding RC limit for this device is only 24GHz.

3.2. Transmission Line characteristics

Fig. 4. Schematic structures for a TWEAM TML. The left figure represent a buried optical waveguide (a.k.a. deeply etched ridge waveguide []) with SI-InP or BCB cladding, the right figure represents an optical ridge waveguide [Coldren] (a.k.a. strip loaded waveguide [17]).

Two typical implementations of TWEAM-TML are illustrated in (Fig. 4) as a buried optical waveguide and ridge waveguide, respectively. A widely used and attractive solution [refs] is the buried optical waveguide with a BCB (or polyamide) cladding. The advantage of this configuration is a low waveguide capacitance, which offers a high characteristic impedance and low electrical attenuation. Due to the high index contrast between BCB and InGaAsP core (1.5/3.4) this implementation is multimode in the horizontal direction. For single mode operation one normally use a semi-insulating (SI) re-grown cladding layer or a ridge waveguide. Single mode operation is actually not required for an electroabsorption modulator [Dagli Wakita], however, it simplifies the process for monolithically integration with a laser. The disadvantage is a higher waveguide capacitance because of the higher dielectric constant of InP and, furthermore, inter-diffusion between *Fe and Zn dopands may degrade the performance of the device. As an alternative, the use of Ruthenium-doped InP* has been successfully demonstrated [2]. The ridge waveguide usually show slightly higher capacitance due to a more divergent electrical field (the charge accumulation close to the lower mesa corners is higher), this capacitance can be improved by adding a small intrinsic buffer layer on top of the active layer (Fig. 4) the resulting capacitance is then close to the value of a buried waveguide (with BCB cladding and the same total intrinsic thickness, h_i). The influence of this additional intrinsic layer will be further discussed in the next section.

The microwave properties of these two implementations are presented in detail in **paper XXX.** The low frequency field solution for the quasi-TEM mode is often referred to as a slow

wave mode [33][34][35]. This type of mode arises due to the physical nature of semiconductor material; the skin-depth of the material is typically very large (e.g. $\delta=8.3\mu m$ at 100GHz for n-InP $10^{18}/cm^3$) and can therefore be treated as a dielectric material for the magnetic-field, whereas the displacement current in the doped semiconductor is typically negligible (e.g. $\omega\varepsilon/\sigma=0.05$ at 100 GHz for p-InP $10^{18}/cm^3$) and is therefore treated as a conductor for the electric field. This leads to a typical EM-field solution illustrated in (Fig. 5). As a result from the influence of the semiconductor material the LC product is much larger than for a conventional TML on an insulating dielectric substrate. The wave propagation is therefore significantly slower than expected from the dielectric constant of the materials used in the structure.

Fig. 5. Transversal field solution in the low-frequency regime, the solid and dashed lines correspond to the electric and magnetic field, respectively.

The TML microwave properties are represented by the quasi TEM circuit model in (Fig. 6). The slow wave mode can be seen as a quasi TEM solution in the sense that the transversal field is dominating over the longitudinal, and the corresponding impedance (Zs) admittance (Yp) per unit length of the TML (Fig. 6) is well described from static field solutions. This is the subject of paper xxx, where we derive the corresponding circuit elements from geometry and material properties. The corresponding TML parameters is expressed as:

$$Z_0(\omega) = \sqrt{\frac{Z_s(\omega)}{Y_p(\omega)}}$$

(3.1)

$$\gamma(\omega) = \alpha(\omega) + j\beta(\omega) = \sqrt{Z_s(\omega)Y_p(\omega)}$$

(3.2)

where

$$Z_s(\omega) = j\omega L + (R_C + R_{CG}) + \omega^2 \frac{L^2}{R_{SC}},$$

(3.3)

$$Y_p(\omega) = \frac{j\omega C_{int}}{1 + j\omega C_{int}R_p} + j\omega C_{ext}$$

(3.4)

Besides the transversal field components the electrical field will also have a longitudinal component (E_z), given by Maxwell's equations:

$$\nabla_T E_z = -j\omega\mu\hat{z}\times\overline{H}_T - \gamma\overline{E}_T \qquad (3.5)$$

This residual E_z component will induce a longitudinal current in the semiconductor material, leading to increased microwave loss at higher frequencies. This leads to the additional R_{SC} circuit element, which is not included in a simple static field solution.
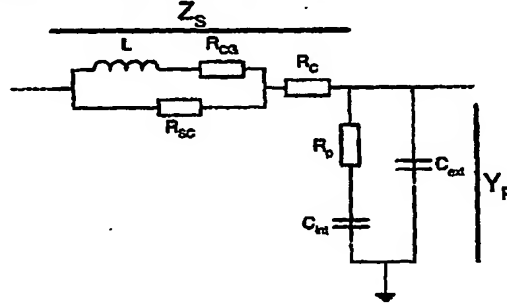

Fig. 6. Equivalent circuit for a unit length of the transmission line.

To understand the tendency of how the TLM parameters scales with geometry it is useful to approximate them with the dominating circuit elements [37]:

$$Z_0 \approx \sqrt{\frac{L}{C_{tot}}} \ ; \quad \beta \approx \omega\sqrt{LC_{tot}} \qquad (3.6a)$$

$$\alpha \approx \frac{R_c + R_{ct}}{2Z_0} + \frac{\omega^2}{2}\left(C_{int}^2 R_p Z_0 + \frac{L^2}{R_{SC}Z_0}\right) \qquad (3.6b)$$

3.3. Small signal performance

This section treats the small-signal bandwidth limitation of a TWEAM, and discusses some possible...

The small signal response of a TWEAM is approximated with the following expression [37]:

$$P_{ac}(t) \propto \int_0^L V_{ac}(z,t)dz \qquad (3.7a)$$

$$V_{ac}(z,t) = \frac{V_0 T e^{j\omega\left(t-\frac{n_e z}{c_0}\right)}}{1 - \Gamma_L \Gamma_S e^{-2\gamma L}}\left(e^{-\gamma z} + \Gamma_L e^{\gamma(z-2L)}\right)\frac{1}{1 + j\omega C_{tot} R_p} \qquad (3.7b)$$

This expression includes the effect of velocity mismatch (n_o), electrical TML attenuation (γ), electrical reflection at the TML source and termination (Γ_S, Γ_L), and the effect of a potential drop over the serial resistance (R_p). All four effects are essential to take into consideration when

the optical response should be determined. In the following section the influence of each effect will be discussed.

b) Velocity mismatch

The velocity mismatch is traditionally often of primal interest when discussing traveling wave structures, *this is probably an inheritance from electro-optical modulators*. Due to the highly attenuating p-i-n configuration electro-absorption modulators are typically short compared to the electrical wavelength ($l<\lambda/2$) within the frequency limit of interest. The name "traveling-wave" is therefore somewhat misleading (traditionally speaking) as the devices are not several wavelengths long, it is however important to realize that the devices are generally too long to be modeled as lumped elements and is ideally operated with an electrical wave only in the forward direction. For a typical structure the electrical index (n_e) is usually slightly more than 5, which indicates a slower propagation of the electrical wave than the optical wave ($n_o\approx3.4$). This walk-off will degrade the performance slightly, but it is generally not a limiting factor.

It is possible to match the propagation velocities of the electrical and optical wave by designing for a lower value of either the capacitance or inductance. The capacitance is however normally given by the optical waveguide design, i.e. the capacitance is chosen as low as possible without significantly sacrifice the optical properties of the device (see next section). This leaves the inductance as the only free parameter to optimize the design with respect to velocity matching. Fundamentally,

$$n_e = c_0 Z_0 C \cdot \tag{3.8}$$

Which indicates the trade-off between velocity matching and TML impedance. In paper **XXX** we have experimentally investigated how the microwave properties is changed with a varying inductance, here the value of the inductance is changed by varying the electrode width.

c) TML attenuation

The effect of TML attenuation is normally dominating over the velocity mismatch. With a negligible velocity mismatch and perfect line termination, the bandwidth is given as:

$$\frac{\left(1-e^{-\alpha L}\right)}{\alpha L} = \frac{1}{\sqrt{2}} \quad \text{or} \quad \alpha L = 0.738 \tag{3.9}$$

Which is equivalent to a TML attenuation of 6.4dB. The attenuation and propagation velocity are however related from the cross product between the real and imaginary part of Z_s and Y_p (3.2), respectively, as indicated by (3.6). Thus a slow propagation is here equivalent to a high attenuation. Therefore (3.8) is important also for the attenuation, and indicates that a high bandwidth design does inevitably result in a low modulator waveguide impedance. **(Inductance)**

d) Impedance mismatch

The TML termination (Z_L) has a very strong effect on the device bandwidth; there are two reasons for this. First, similar as for a lumped (RC-limited) modulator, the value of Z_L sets the normalized DC-response, a simple way to achieve a high bandwidth is to lower the DC-response

(with a constant response at high frequencies). The second reason is that in the TWEAM configuration the load impedance is transformed, a typical modulator length close to the 3dB-bandiwth is $l \approx \lambda/4$, thus the impedance seen at the input of the modulator is approximately $Z_{IN}=Z_0^2/Z_L$. With $Z_L<Z_0$ the input impedance (and the voltage at the modulator input) will increase with frequency, and thereby increase the response at higher frequencies. Due to the impedance transformation the load impedance has a stronger effect on the bandwidth for the TW-configuration than for a lumped (RC-limited) modulator. This is a very effective way to increase the bandwidth of the device, but it is also important to realize that with $Z_L>Z_0$ the bandwidth will be significantly reduced due to the same effect. It is therefore good to design with slightly to low than to high load impedance. The effect of bandwidth peaking is obviously dependent on the source impedance, e.g. if a $Z_S=50\Omega$ source or dedicated driver design is used. Only if the TWEAM is matched $(Z_L=Z_0)$ the input impedance is almost frequency independent, and the bandwidth is independent of the source impedance.

e) Internal RC limitation

Due to the low conductivity of p-InP the voltage over the intrinsic layer is lower than the voltage on the modulator electrode, this indicates an internal RC-constant given by R_pC_{int}. In a successful process this should typically not be a dominating effect below approximately 200GHz, in a practical process due to unintentional low doping or passivation of dopands this can have pronounced effects already at lower frequencies. In our earlier results (paperXXX) the internal RC-limit corresponded to only about 60GHz, the bandwidth could only be increased over this limit by designing with a low Z_L.

3.4. Optimization of the intrinsic layer thickness and large-signal extinction

An important design parameter for the TW-design is the possibility to make the intrinsic layer thicker than the optical waveguide as illustrated in (Fig. 4). The thickness of the optical waveguide is limited to maintain single-mode operation, and/or can be restricted by the number of wells in a QW-design with respect to carrier transport and material quality... Increasing the thickness of the intrinsic layer will obviously reduce the electrical field for a fixed applied voltage, and thereby reduce the strength of the electro-optical (EO) interaction. However, the performance of a traveling-wave modulator does not scale with geometry in the same way as a lumped (RC-limited) modulator. This changes the optimum design with respect to the intrinsic layer thickness of the modulator (Fig. 4) and its corresponding waveguide capacitance (C_{int}). For example: for a lumped modulator the bandwidth is directly proportional to the capacitance, decreasing this value (per unit length) by a factor of two indicates that the device can be made twice as long and still have the same bandwidth. For a matched TW-design $(Z_L=Z_0)$ the bandwidth is given by the αL product (3.9), and with a thin intrinsic layer α is proportional to $C_{int}^{(3/2)}$ (3.6). Hence, reducing C_{int} with a factor of two indicates that the device length can be increased by a factor up to 2.8 without decreasing the device bandwidth. In addition the penalty for internal RC limitation and velocity mismatch are reduced, and the characteristic impedance is increased. This indicates that a TW-design benefits from a long modulator with weak EO interaction, i.e. thick intrinsic layer.

The thickness of the intrinsic layer has a large effect on the general modulator performance with respect to optical extinction, high power saturation and frequency chirp. A detailed optimization is therefore complicated.

Generally a thicker intrinsic layer is beneficial for the following reasons:

+ Decreased capacitance, which leads to decreased attenuation, increased impedance, and decreased internal RC-penalty. The modulator length can be increased without reducing the small signal BW.

+ The optical absorption per unit length is reduced; a more distributed optical absorption decreases the effect of high power saturation related to the carrier escape time from the QW.

+ Decreased free carrier absorption from p-dopands [ref].

+ Decreased diffusion of p-dopands into the MQW layer in MOVPE growth [ref]

The drawback of a long modulator with a thick intrinsic layer is mainly associated with high power saturation and frequency chirping as:

− The carrier drift time is increased due to the thicker i-layer, this may increase the high power saturation due to carrier screening [value approx $7*10^6$ cm/s according to monte carlo ref?].

− Hole pile-up [ref olof mm] in the bandgap discontinuity may be an issue unless treated with proper bandgap engineering.

− The frequency chirp-parameter $(C=2\Delta n/\Delta \alpha)$ [41] is usually lower with a high electrical field Kolla Myazaki.

− The insertion loss may be increased depending on the low-field absorption.

− Non-intentional residual doping in the intrinsic region may increase the drive voltage.

To further investigate the optimum design with respect to optical extinction we use the case study corresponding to a ridge waveguide (Fig. 4) with parameters...

A smaller mesa leads to a decreased optical confinement and potentially increased scattering losses from sidewall imperfections.

and a design bandwidth of 100GHz. Fig. 7 shows how the TML parameters are affected by an additional intrinsic layer thickness, the parameters are calculated using a slightly modified version of the model in paper XXX. As illustrated a reduced C_{int} has a strong influence of the modulator TML attenuation (α), furthermore the characteristic impedance (Z_0) is increased and the velocity matching is improved.
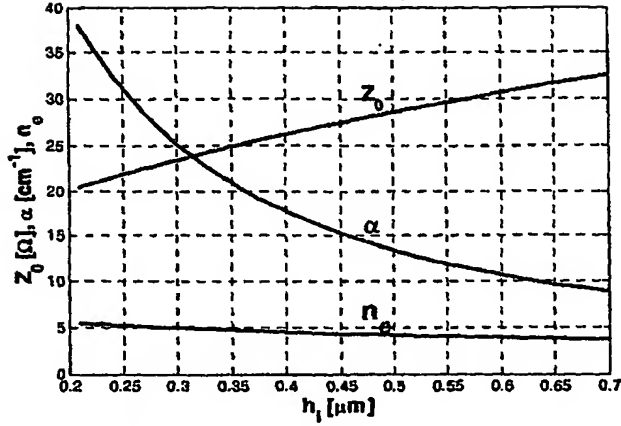
Fig. 7. TML parameters at fq=100GHz as a function of intrinsic layer thickness for a ridge-mesa waveguide with a width of 1.5μm.

With the TML parameters given by (Fig. 7) we can calculate the corresponding modulator length that corresponds to a fixed small signal bandwidth for a matched TWEAM using (3.7), for this case study (Fig. 9) shows the corresponding length for 100GHz bandwidth.

As figure of merit (FOM) for the optimization we use the large signal optical extinction ratio (ER=10log(P_0/P_I)) given the modulator drive voltage (ΔV). The extinction ratio is proportional to the optical attenuation (α_0) resulting from the electric field corresponding to a sent "1" or "0" symbol (E_I, E_0).

$$\log(ER) \propto \left(\alpha(E_1) - \alpha(E_0) \right)l$$

Empirically the optical absorption difference can be expressed by the following curve fit (Fig. 8):

$$\Delta\alpha = p\left(E - E_0\right)^c = p\left(\frac{V - V_0}{h_i} \right)^c$$

Where the proportional parameter (p) and curvature parameter (c) are fitting parameters. The important parameter for device optimization is the curvature parameter (c) that is given by material, low field bias (E_0 or V_0), and wavelength detuning (the examples in (Fig. 8) also includes additional optical losses). Note that the value of the curvature parameter is strongly related to a tolerated insertion loss, i.e. a high c value is equivalent to the case when the modulator is operating well into the nonlinear region in the transmitting state (Fig. 8).
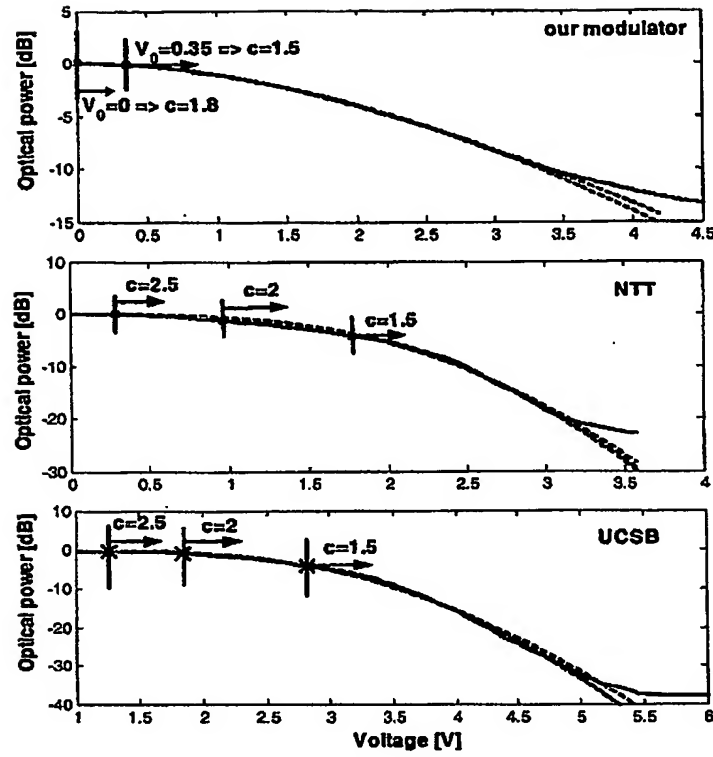
Fig. 8. Example of model fit for InGaAsP/InGaAsP QW devices with corresponding curvature parameter (c) applied to our modulator structure, NTT [49], and UCSB [48] respectively.

The traditional FOM [refs] use the drive voltage from a 50Ω source rather than the actual drive voltage applied to the modulator.

$$V_m = V_{50} \frac{2Z_0}{50 + Z_0}$$

A perhaps more fundamental FOM is to optimize the optical extinction with respect to applied modulation signal power as:

$$V_m = \sqrt{Z_0 P_{sig}}$$

The resulting relative extinction given from the expression

$$\log(ER) \propto \left(\frac{\Delta V_m}{h_i} \right)^c l(h_i)$$

are plotted in (Fig. 9) for both cases with a fixed voltage, using curvature parameter ($c=1.5$, 2.0 and 2.5).

Fig. 9. The upper figure shows the modulator length resulting in 100GHz BW as a function of intrinsic layer thickness. The lower figures show the corresponding relative change for the extinction in dB (i.e. if 1 corresponds to 10dB ER then 0.5 corresponds to 5dB ER) for a fixed drive power and fixed voltage from a 50Ω source, respectively. Note that the thickness of the active layer (0.2μm) and the optical confinement is here assumed constant.

As illustrated, the optimum thickness is dependent on the assumed curvature parameter value. If a low c value can be tolerated, with respect to the insertion loss, it is obvious that the large signal extinction is improved using a thick intrinsic layer and long modulator for the TW design. On the other hand, the trend is that the longer modulator the higher c value is probably required in order to limit the insertion loss, and the opposite hold for a short modulator. Therefore, it is very difficult to argue for the most optimal design. However, the result in (Fig. 9) indicates that a thickness of 0.3 to 0.4 μm with a corresponding modulator length of approximately 200 to 300 μm is a good value for a design bandwidth of 100GHz. For a low c value we find that the intrinsic layer can be made very thick without sacrificing the optical extinction. This is interesting for a high modulator impedance design; however, the trade-off with insertion loss and frequency chirp indicates that a design with much thicker i-layer than 0.5μm is not feasible. The characteristic impedance is therefore in practice limited to approximately 30Ω (Fig. 7).
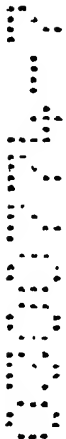
4. Optimization of high impedance modulators

Due to the current standard of microwave systems modulator impedances in the proximity of 50Ω is preferred. This is significantly higher than the typical TWEAM design [ref] with a characteristic impedance usually between 20 and 25Ω. It is not fundamentally impossible to design a modulator with higher impedance, however, as illustrated in the previous chapter it is not optimal to use an intrinsic layer much thicker than approximately 0.5μm. With a mesa width of 1.5μm this corresponds to a WG capacitance of approximately 500pF/m or a characteristic impedance slightly less than 30Ω (with a typical inductance of L≈400nH/m, figure 10 in **paper XXX**). The capacitance can be reduced slightly by increasing the i-layer thickness and reducing the mesa width, this is however limited by the trade-off with respect to optical performance of the modulator. Increasing the value of the inductance further increases the penalty from velocity mismatch (3.8) and TML attenuation, the latter arises partly from the practical problem of increasing the inductance without increasing the dissipative elements in the Z_S network in (Fig. 6) but also from the resulting cross product with the dissipative element in the Y_P network in (3.2 or 3.6).

Two attractive ways to solve this problem is either to match the modulator to the source and load with a passive network, e.g. a taper (Fig. 10) [38],[18], or to effectively reduce the capacitance per unit length by dividing the modulator into several segments (Fig. 2), i.e. a periodic capacitive loaded TML [43],[45],[46]. There is a clear distinction between the two regimes: In order to effectively transform the impedance the required taper length should be more than $l > \lambda/4$, while for the segmented TML matching (Fig. 2) the length of the segments should typically be less than $l < \lambda/4$.

4.1. Taper matching of traveling wave modulators

A schematic representation of a taper matching is illustrated in (Fig. 10). The ideal taper transforms the modulator impedance level of 25Ω to the standard level of 50Ω. The use of tapers to embed the modulator in a 50Ω environment is discussed in the work by Zhang [18], although the final implementation in this work is more related to a single segmented TML matching (Fig. 2).
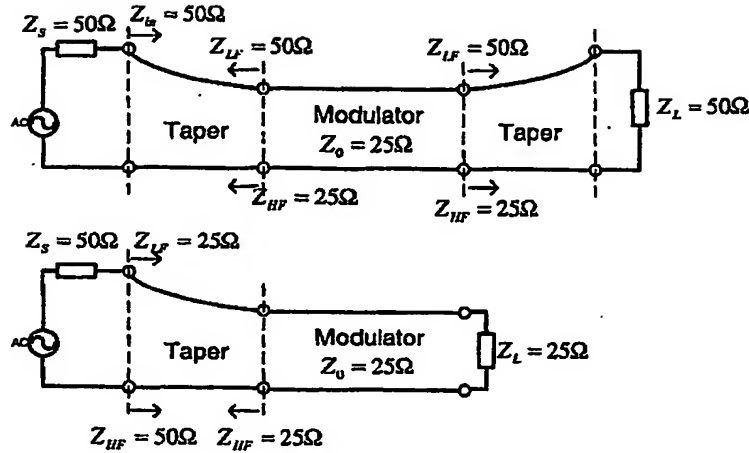
Fig. 10. Schematic representation of 50Ω impedance matching using passive waveguide tapers [collin]. The upper circuit shows a configuration with input and output matching of the modulator; the input impedance can thereby be matched to 50Ω also at low frequencies. In the lower figure the output taper is replaced with a 25Ω matching resistor, this results in a source mismatch (Zin≠50Ω) at lower frequencies.

The practical problem with taper matching is the low-frequency performance, unless the taper is infinitely long. At low frequencies the taper does not affect the electrical signal, and the modulator is then terminated with 50Ω (Fig. 10, upper circuit). Above a designed transition frequency (f_t) the taper will ideally transform the modulator impedance of 25Ω to the system impedance of 50Ω. There are generally two problems associated with this implementation. First, in order to keep the transition frequency sufficiently low the taper requires quite large chip area in a practical implementation. For example: λ/4-transformer $(l≈λ/4)$, exponential taper $(l≈λ/2)$, and triangular taper $(l≈0.815λ)$ [collin]. With an implementation as a CPW on SI-InP $(n_e≈2.6)$ the required taper length can easily be several millimeters in order to have a transition frequency in the relevant region (say 10GHz or lower). The second problem is that not only the impedance will be transformed but also the applied voltage to the modulator. Considering the two-taper implementation (Fig. 10, upper circuit) the resulting modulator voltages are:

$$V_{mLF} = \frac{V_g}{2} \quad , \text{ while } \quad V_{mHF} = \frac{V_g}{2}\sqrt{\frac{25}{50}} = \frac{V_{mLF}}{\sqrt{2}} .$$

Thus the voltage transformation alone limits the 3dB bandwidth for the configuration with two tapers. This configuration is therefore not useful for a wideband application (e.g. NRZ modulation) unless the transition frequency is designed to a very low frequency. (Or sufficiently high frequency, but this obviously means that the tapers are not effectively used).

For the single taper implementation (Fig. 10, lower circuit) the resulting voltages are:

$$V_{mLF} = \frac{25}{50+25}V_g = \frac{V_g}{3} \quad , \text{ while } \quad V_{mHF} = \frac{V_g}{2}\sqrt{\frac{25}{50}} = \sqrt{\frac{9}{8}}V_{mLF} .$$

Thus the voltage applied to the modulator is here almost frequency independent (within 0.5dB), and there is no BW penalty from the taper. Hence this implementation can be used also for

wideband applications. The transition frequency is not critical for the modulator performance (S_{21}) but it affects the input reflection of the device (S_{11}). Also note that the bandwidth is maintained because the LF response is *reduced* due to the impedance mismatch, the HF response is the same as for the two-taper implementation.

4.2. Periodic segmented TML traveling wave structures

f) Introduction to periodic structures

A more compact approach of impedance matching is to effectively reduce the capacitance per unit length by dividing the modulator into several segments separated by passive (high impedance) electrode segments (Fig. 11). As long as the segments are sufficiently short compared to the electrical wavelength, in the frequency range of interest, the electrical wave will "see" the "average" impedance given by each TML impedance and segment length (see next section). This implementation is often referred to as a periodic traveling wave structure [collin] or capacitively loaded TML [43], [45]. By choosing the appropriate impedance value of the passive WG and segment length ratio it is possible to design with perfect impedance and velocity matching (eq. 4.5).
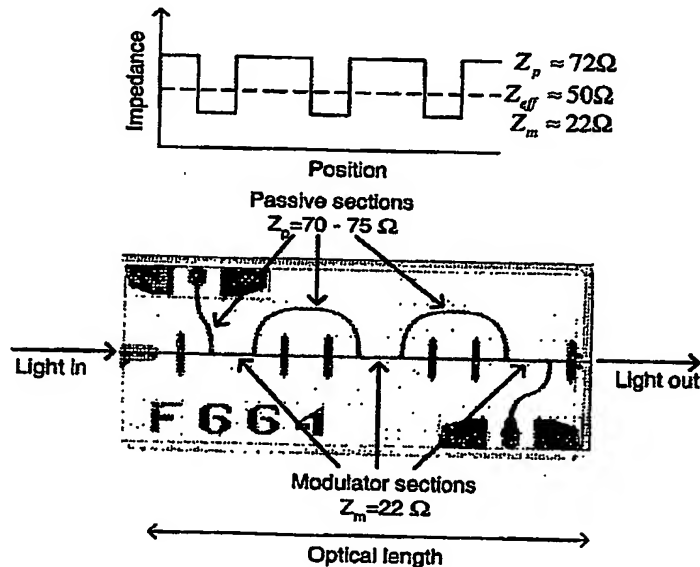

Fig. 11. Layout of a periodic traveling wave modulator structure. The modulator is here divided into 3 sections, each with a length of 50μm. Passive sections used to increase the effective characteristic impedance separate the modulator sections.

This matching technique has been demonstrated for electro-optic modulators [20]-[46]. Also the extreme case of using only one modulator segment between two passive segments with high impedance can be included in this category. This has been demonstrated for electro absorption

modulators, designated impedance controlled electrode (ICE) modulator [13]. The technique has however been demonstrated in earlier work, for example in the work by Zhang [18] the "Linear width taper" can be considered to operate within this regime (see figure 3.27 to 3.30 in [18]). Basically there are two different implementations used in the literature (Fig. 12):

    a)   Cascaded segments alternating between low impedance active modulator and passive high ohmic segments. This approach is used in this work (Fig. 11) and in ref. [46].

    b)   A continuous passive high ohmic WG where the signal is feed to short lumped modulator segments via an inductive feed line [20],[45].

In our work a conductive substrate was used for compatibility with laser integration (available SI-substrates typically show more crystal defects that degrades the lifetime reliability of the laser [ref?]). The use of a conductive substrate limits the freedom of design for the passive electrode, and alternative a) was chosen primarily for layout reasons. There are however two advantages with this implementation, first the inductance of the modulator segment is effectively used (in alternative b the modulator segments only add to the capacitance), secondly the inductive feed line increases the admittance per unit length

$$Y_{pB} \approx \frac{j\omega C_m}{1 - \omega^2 L_{feed} C_m}.$$ (4.1)

This increase leads to a decreased Z_0, which potentially degrades the device performance at higher frequencies.
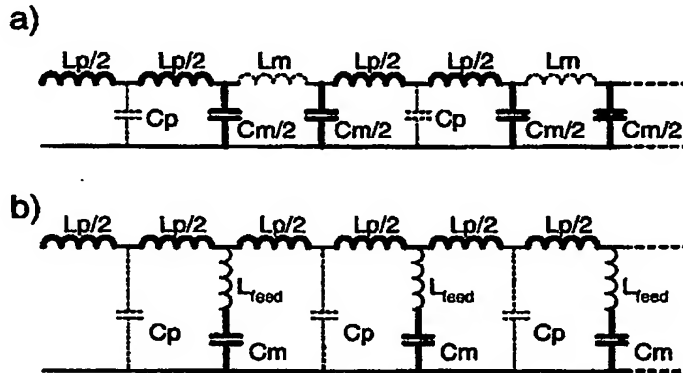

Fig. 12. Two types of implementation of segmented modulators: a) The cascaded approach used in this work (Fig. 11) and in [46], b) The inductive feed line approach used by e.g. Walker [43].
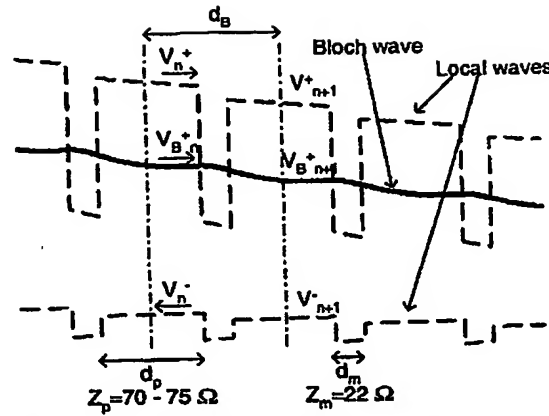
g) Bloch Wave Formalism

Fig. 13. Bloch wave representation for an infinitely long (or matched) periodic TML. The plot shows the amplitude as function of position for the forward propagating wave (V^+), reverse propagating wave (V^-), and the resulting forward propagating Bloch wave (V_B^+).

The wave propagation for a periodic TLM can be expressed in form of Bloch waves [38] (Fig. 13) with its associated TLM parameters γ_B and Z_B. The wave propagation on an infinite (or matched) structure between sampled points separated by the length of the periodicity (d_B) is then given as:

$$V_{Bn}^+ = V_n^+ + V_n^- = V_{B0}^+ e^{-\gamma_B n d_B} \tag{4.2}$$

The Bloch wave representation is interesting as it corresponds to the effective characteristic impedance and propagation factor extracted from measured S-parameters (chapter **Error! Reference source not found.**). The propagation factor is derived from the T-matrix of a unit cell of the periodic structure:

$$\begin{pmatrix} V_n^+ \\ V_n^- \end{pmatrix} = \begin{pmatrix} T_{11} & T_{12} \\ T_{21} & T_{22} \end{pmatrix} \begin{pmatrix} V_{n+1}^+ \\ V_{n+1}^- \end{pmatrix} = \begin{pmatrix} e^{\gamma_B d_B} & 0 \\ 0 & e^{\gamma_B d_B} \end{pmatrix} \begin{pmatrix} V_{n+1}^+ \\ V_{n+1}^- \end{pmatrix} \tag{4.3}$$

The resulting propagation factor is given from the trace of the matrix, i.e., $\cosh(\gamma_B d_B)=(T_{11}+T_{22})/2$. The Bloch impedance for a symmetric structure is then given as:

$$\Gamma_B = \frac{V_n^+}{V_n^-} = \frac{T_{11} - e^{\gamma_B d_B}}{T_{12}}, \text{ and } Z_B = \frac{V_n}{I_n} = Z_P\left(\frac{V_n^+ + V_n^-}{V_n^+ - V_n^-}\right) = Z_P\left(\frac{1+\Gamma_B}{1-\Gamma_B}\right). \tag{4.4}$$

h) Properties of periodic structures

In the low frequency limit ($\lambda_0 \ll n_B d_B$) the Bloch impedance and propagation factor corresponds to the average impedance of the two TML sections:

$$Z_{B,LF} \approx \sqrt{\frac{Z_{xp}d_p + Z_{sm}d_m}{Y_{pp}d_p + Y_{pm}d_m}} , \quad \gamma_{B,LF} \approx \sqrt{\left(Z_{xp}\frac{d_p}{d_B} + Z_{sm}\frac{d_m}{d_B}\right)\left(Y_{pp}\frac{d_p}{d_B} + Y_{pm}\frac{d_m}{d_B}\right)} \quad (4.5)$$

Where Z_{sn} and Y_{pn} is the corresponding impedance and admittance per unit length of each TML, respectively. Ideally Z_B and γ_B are then only dependent on the ratio between the active and passive waveguide length (d_p/d_m), and independent on the periodicity of the structure (d_B) (Fig. 14). (In practical implementations each waveguide transition will wave discontinuities that act as parasitic circuit elements, this effect is not included in the simulations presented in this chapter).

Fig. 14. Measured and simulated Bloch TML parameters for structures with different periodicity using the same ratio of d_n/d_p and a total modulator length of 150μm. The propagation factor is normalized to the optical path length. The simulations uses TML parameters extracted from measurements on straight test-structures for each TML type respectively.

There is however an upper frequency limit when Z_B and n_B becomes frequency dependent (Fig. 14), once the segment length is comparable to (half) the electrical wavelength a stop-band will occur (Fig. 15) (a.k.a. band-gap or Bragg-frequency) [38]. Due to the TML losses the stop-band will not be complete for these modulator structure (i.e. the eigenvalue equation for the propagation factor (4.3) will have a solution also in the stop-band region). In practice, because of high attenuation and dispersion, the structure is only useful up to the stop-band edge given by the spatial repetition rate of the TML segments.

A very interesting effect is that close to the stop band edge a standing wave pattern arises in the structure. Fig. 15 illustrates the voltage difference between a structure with dense segmentation and one with a coarse segmentation close to the stop-band edge. The coarse segmentation show a higher attenuation but also an added standing wave pattern. The standing

wave works in favor for the modulation efficiency as the antinodes of this pattern is situated in the low impedance TML sections (i.e. the modulator sections), this voltage increase peaks the transfer function and compensates for the higher attenuation and impedance decrease that arises close to the band-edge (Fig. 14). This indicates that the device can be designed with a BW slightly less than the actual band edge, at higher frequencies the transfer function will fall off rapidly. The standing wave pattern should not be too pronounced as this may result in a non-linear phase response in the transfer function. Note that this is a local standing wave effect, the voltage phase difference between each modulator section is significantly less than π. This would otherwise correspond to the center of the stop-band. This standing-wave effect should not be confused with the standing-wave enhanced operation mode proposed by UCSB [ref PTL] for short pulse generation or OTDM demultiplexing.

In a practical design it is desirable to reduce the number of segments as much as possible. The main reason for this is that the optical path length of the device is thereby minimized (Fig. 11); this reduces the insertion loss of the device. For example with only one modulator segment the effective modulator length and optical path length is the same, with two modulator sections only one passive section is adding to optical path length, and so on. The number of segments should therefore be chosen so that the stop-band edge occurs at a slightly higher frequency than the corresponding attenuation limited bandwidth (see Fig. 16). Typically, with an effective modulator length of 200μm only one segment is required to operate in the 40GHz regime, while 2 or 3 segments are needed to operate in the 100GHz regime (Fig. 14).
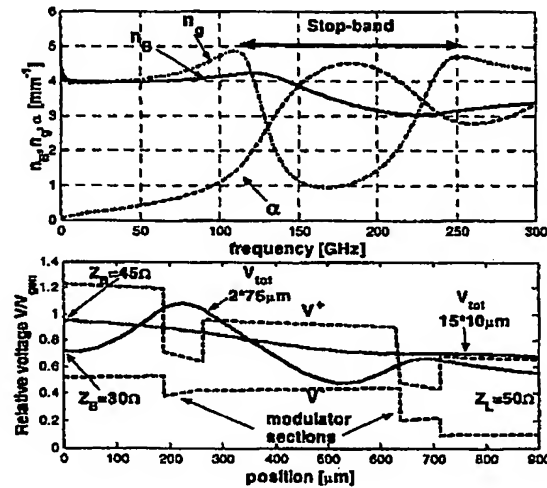

Fig. 15. Upper figure shows the simulated frequency dependence of the phase-index, group-index, and attenuation of the Bloch wave for a 2*75μm modulator structure. The lower figure illustrates the standing wave pattern that appears close to the stop band edge (100GHz). Also included is the corresponding voltage for a structure with a dense segmentation (15*10μm).

i) Design optimization of a segmented structure

Although the TML attenuation is reduced as an effect of the reduced capacitance per unit length, the device length has to be increased to retain the same effective modulator length. The attenuation normalized to the effective modulator length will always be increased with higher impedance. The theoretical attenuation limited bandwidth given with our extracted TML parameters ($C_{mod} \approx 650$pF/m, $Z_{passive} \approx 75\Omega$) is plotted in (Fig. 16). This bandwidth corresponds to a structure with a high repetition rate resulting from (4.5) with (3.7), assuming perfect line termination, and velocity matching. Note that the velocity matching can easily be adjusted for a segmented TML by making the electrical TML longer than the optical WG (Fig. 11).
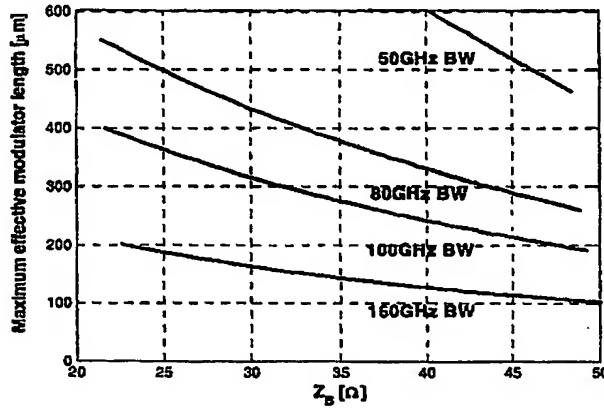

Fig. 16. Length impedance tradeoff in the attenuation limit with perfect line termination and, velocity matching.

The obvious gain of the higher impedance of a segmented structure is a reduced return loss (S_{11}) to a 50Ω system. It is however clear from Fig. 16 that the higher impedance comes only with the price of a reduced modulator length, and thereby increased (modulator) drive voltage. It is therefore relevant to investigate the trade-off between large-signal optical extinction and impedance level. Here I use the same approach as in section (3.4) and relate the extinction to the curvature parameter of the absorption curve (Fig. 8). This is done for three different reference cases:

a) The extinction is optimized with respect to the voltage from a 50Ω source. The modulator voltage is here given as:

$$V_m = V_{50} \frac{2Z_0}{50 + Z_0}$$

b) The extinction is optimized with respect to the drive current. This situation is also relevant when a high input impedance close to 50Ω is important, for example in order to make the device less sensitive to a parasitic inductance in an interconnect (e.g. bond-wire or flip-chip bonding). A very simple way to solve this problem is to add a serial

resistor so that the input impedance always is 50Ω. The modulator voltage is here given as:

$$V_m = V_{50} \frac{2Z_0}{50 + Z_0 + R_{serial}} = V_{50} \frac{Z_0}{50} \propto Z_0 I_{source}$$

c)   The extinction is optimized with respect to drive power:
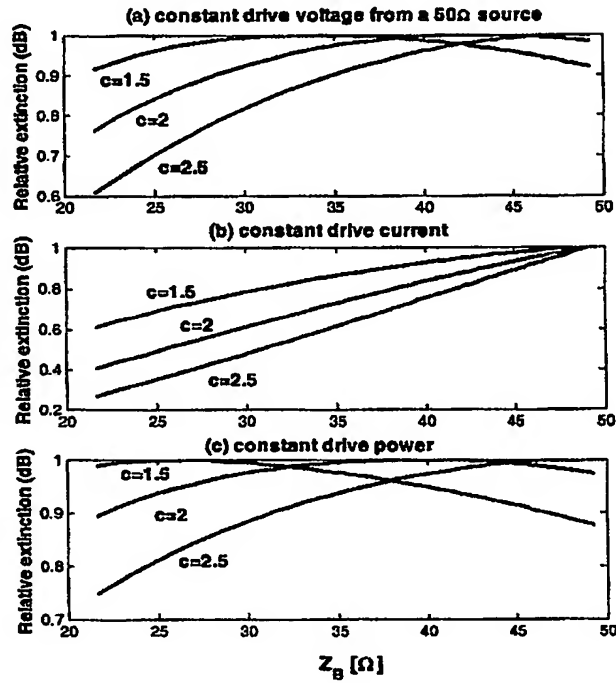
$$V_m = \sqrt{Z_0 P_{sig}}$$

Fig. 17. Large signal optical extinction trade-off for three different drive configurations as a function of the Bloch impedance. The design corresponds to the 100GHz BW curve in Fig. 16. The figures show the relative change of the logarithmic extinction (i.e. if 1 corresponds to 10dB extinction then 0.5 corresponds to 5dB extinction).

This case study for 100GHz devices illustrated in Fig. 17 indicates that if a high input impedance is important it is clear that a segmented TML approach should be used rather than a serial resistive matching element. However, for the cases of a 50Ω source or optimised drive power the modulator impedance should be designed close to 35Ω rather than 50Ω, provided that the return loss can be relaxed to $S_{11} \approx -15$dB (unless a high curvature parameter (c) value is used).

5. References

[1] hgfhdd

[2] M. Tamura, T. Yamanaka, H. Fukano, Y. Akage, Y. Kondo, T. Saitoh, "High Speed Electroabsorbtion Modulators Using Ruthenium-Doped SI-InP: Impact of Interdiffusion-Free Burying Technology on E/O Modulation Characteristics", *Proceedings of IPRM 2003*, Santa-Barbara, Carlifornia, 2003.

[3] T. Ido, S. Tanaka, M. Suzuki, M. Koizumi, H. Sano, H. Inoue, "Ultra-High-Speed Multiple-Quantum-Well Electro-Absorption Optical Modulators with Intrgrated Waveguides", *IEEE J. Lightwave Technol.*, vol. 14, no. 9, pp 2026-2034, Sep. 1996.

[4] F. Devaux, S. Chelles, A. Ougazzaden, A. Mircea, and J. C. Harmand, "Electroabsorption modulators for high-bit-rate optical communications: a comparison of strained InGaAs/InAlAs and InGaAsP/InGaAsP MQW", *Semicond. Sci. Technol*, vol. 10, no. 7, pp 887-910, July 1995.

[5] D. G. Moodie, A. D. Ellis, P. J. Cannard, C. W. Ford, A. H. Barrell, R. T. Moore, S. D. Perrin, R. I. McLaughin, F. Garcia., "40Gbit/s modulator with low drive voltage and high optical output power", *European conference on optical communication ECOC 2001*, pp 332-333, 2001.

[6] N. Mineo, K. Nagai, T. Ushikubo, "Ultra wide-band electroabsorption modulator modules for DC to millimeter-wave band", *Microwave Photonics 2001. MWP '01.* pp 9-12, 2002.

[7] X. Fu, T. Liu, J. Li, and G. Zhang, "Investigation of Electroabsorption Modulator for 40Gb/s Transmitter Application", *Optical fibre conference OFC 2002*, pp 718-719, 2002.

[8] Lumped tuned H. Feng, T. Makino, S. Ogita, H. Maruyama, and M. Kondo, "40Gb/s Electro-absorption Modulator Integrated DFB Laser with Optemized Design", *Optical fiber conference OFC 2002*, pp 340-341, 2002

[9] H. Tada, Y. Miyazaki, K. Takagi, T. Aoyagi, T. Nishimura, and E. Omura, "40 GHz Modulation Bandwidth of Electroabsorption Modulator with narrow-mesa ridge waveguide", *Optical fibre conference OFC 2002*, pp 722-723, 2002.

[10] Y. Miyazaki, H. Tada, S. Tokizaki et.al., "Small chirp 40Gbps EA modulator with novel tensile-strained asymmetric quantum well absorption layer", *European conference on optical communication ECOC 2002*, paper 10.5.6, 2002.

[11] K. Takagi, Y. Miyazaki, H. Tada, E. Ishimura, T. Aoyagi, T. Nishimura, T. Hatta, E. Omura, "Highly reliable 40Gb/s electroabsorption modulator grown on InP:Fe substrate", *Conference on InP and related materials IPRM 2001*, pp 432-435.

[12] B. Mason, A. Ougazzaden, C. Lentz, K. Glogovsky, et. al. (20 authors), "40-Gb/s Tandem Electroabsorption Modulators", *IEEE Photon. Technol. Lett.*, vol 11, no 2, pp. 27-29, Jan. 2002.

[13] M. Shirai, H. Arimoto, K. Watanbe, A. Taike, K.shinoda, J.Shimizu, H. Sato, T. Ido, T. Tsuchiya, M. Aoki, and T. Tsuji. "Impedance-Controlled-Electrode (ICE) Semiconductor Modulators for 1.3-μm 40Gbit/s Tranceivers", *ECOC 2002 proceedings vol. 4*, paper 9.5.4., 2002.

[14] UCSB TWEAM Y-J Chiu, H-F Chou, V. Kaman, P. Abraham, and J.E. Bowers, "High extinction ratio and saturation power traveling-wave electroabsorption modulator", *IEEE Photon. Technol. Lett.*, vol 14, no 6, pp. 792-794, Jun 2002.

[15] NTT TWEAM Y.Akage, K. Kawano, S. Oku, R. Iga, H. Okamoto, Y. Miyamoto, and H. Takeuchi, "Wide bandwidth of over 50 GHz traveling wave electrode electroabsorption modulator integrated DFB lasers", *Electron. Lett.*, vol. 37, no. 5, pp. 299-300, 2001.

[16] San diego G. L. Li, S. A. Pappert, P. Mages, C. K. Sun, W. S. C. Chang and P. K. L. Yu, "High-Saturation High-Speed Traveling-Wave InGaAsP-InP Electroabsorption Modulator", *IEEE Photon. Technol. Lett.*, vol 13, no 10, pp. 1076-1078, 2001.

[17] Koichi Wakita, *Semiconductor optical modulators*, USA:Kluwer Academic Publishers 1998.

[18] S. Zhang, "Traveling-wave Electroabsorbtion Modulators", University of California, Santa Barbara, CA, Ph. D. Dissertation 1999.

[19] N. Dagli, "Wide-Bandwidth Lasers and Modulators for RF Photonics", *IEEE Trans. Microwave Theory Tech.*, vol. 47, no. 7, pp 1151-1171, July 1999.

[20] R. G. Walker, "High-Speed Semiconductor Intensity Modulators", *IEEE J. of Quantum Electron.*, vol. 27, no. 3, pp 654-667, 1991.

1,21 28

[21] LiNbO3 K. Noguchi, O.Mitomi, and H. Miyazawa, "Millimeter-Wave Ti:LiNbO₃ Optical Modulators", *IEEE J. Lightwave Techn.*, vol. 16, no. 4, april 1998.

[22] W. Wang, D. Chen, H. Fetterman, Y. Shi, W. Steier, L. Dalton, P-M. Chow, "Optical heterodyne detection of 60 GHz electro-optic modulation from polymer waveguide modulators", *Appl. Phys. Lett.*, vol. 67, no. 13, pp. 1806-1808, 1995.

[23] D. Chen, H. Fetterman, A. Chen, W. Steier, L. Dalton, W. Wang, Y. Shi, "Demonstration of 110 GHz electro-optic polymer modulators", *Appl. Phys. Lett.*, vol. 70, no. 25, pp. 3335-3337, 1997.

[24] D. Chen, D. Bhattacharya, A. Udupa, B. Tsap, H. Fetterman, A. Chen, S-S. Lee, J. Chen, W. Steier, L. Dalton, "High-Frequency Polymer Modulators with Integrated Finline Transitions and Low V.", *IEEE Photonics Tech. Lett.*, vol 11, no. 1, pp 54-56, Jan. 1999.

[25] R. Sahara, K. Morito, K. Sato, Y. Kotaki, H. Soda, N. Okazaki, "Strongly Improved Frequency Response at High-Optical Input Powers from InGaAsP Compensated Strain MQW Electroabsorption Modulators," *IEEE Photon. Technol. Lett.*, vol 7, no 9, pp. 1004-1006, Sep. 1995.

[26] J. Piprek, Y.-J. Chiu, J. E. Bowers,"Analysis of Multi-Quantum Well electroabsorption Modulators," *SPIE Proc. 4646-77, Physics and Simulation of Optoelectronic Devices X, Photonics West*, San Jose, Jan. 2002.

[27] R. G. Walker JLT, "High-Speed Electrooptic Modulation in GaAs/GaAlAs Waveguide Devices", *J. Lightwave Technol.*, vol. 5, no.10, pp. 1444-1453, oct. 1987.

[28] C. C. Teng, "Traveling-wave polymeric optical intensity modulator with more than 40 GHz of 3-dB electrical bandwidth", *Appl. Phy. Lett.*, vol. 60, no. 13, pp1538-1540, march 1992.

[29] NTT Demux, S. Kodoma, T. Yoshihide, H. Ito, "320-Gbit/s Demultiplexing with Monolitic PD-EAM Optical Gate", European conference on optical communication ECOC 2002, paper 8.4.1, 2002.

[30] H-F. Chou, Y-J. Chiu, J. E. Bowers, L. Rau, S. Rangarajan, and D. J. Blumenthal., "Standing-wave Enhanced Electroabsorption Modulator for 80Gb/s to 10Gb/s OTDM Demultiplexing", Proc. ECOC 2002, vol. 3, session 8.4.6.

[31] Semiconductor Light Sources for 40-Gb/s Transmission Systems
Kenji Sato ;
Journal of Lightwave Technology : Accepted for future publication , 2002
Page(s): 1

[32] SLOW

[33] Y. R. Kwon, V. M. Hietala, K. S.Champlin, "Quasi-TEM Analysis of "Slow-Wave" Mode Propagation on Coplanar Microstructure MIS Transmission Lines", *IEEE Trans. Microwave Theory Tech.*, vol. MTT-35, no. 6, pp. 545-551, June1987.

[34] H. Hasegawa, M. Furukawa, H. Yanai, "Properties of Microstrip Line on Si-SiO₂ System", *IEEE Trans. Microwave Theory Tech.*, vol MTT-19, no. 11, pp 869-881, nov 1971.

[35] Y. Fukuoka, Yi-Chi Shih, and T. Itoh, "Analysis of Slow-Wave Coplanar Waveguide for Monolithic Integrated Circuits", *IEEE Trans. Microwave Theory Tech.*, vol MTT-31, no. 7, pp 567-573, July 1983.

[36] GENERELLA

[37] G. L. Li, S. K. Sun, S. A. Pappert, W. X. Chen, and P. K. L. Yu, "Ultrahigh-Speed Traveling-Wave Electroabsorption Modulator - Design and Analysis", *IEEE Trans. Microwave Theory Tech.*, vol. MTT-47 , no. 7, pp. 1177-1183, July 1999.

[38] R. E. Collin, *Foundation for Microwave Engineering*, Second edition, Singapore: McGraw-Hill, 1992. Chapter 8.

[39]

[40] SPICE J. Lim, S. Jeon, J. Kim, and S. Hong, "A Circuit Model of Traveling Wave Electroabsorption Modulators", *Microwave Symposium Digest*, vol. 3, pp. 1707 -1710 , 2002.

[41] Chirp F. Koyana, and K. Iga, "Frequency Chirping in External Modulators", *IEEE J. Lightwave Techn.*, vol. 6, no.1, jan 1988.

[42] Chirp exp F.Devaux, Y. Sorel, and J. F. Kerdiles, "Simple Measurement of Fiber Dispersion and of Chirp Parameter of Intesity Modulated Light Emitter", *IEEE J. Lightwave Techn.*, vol. 11, no. 12, dec. 1993.

[43] Periodiska:

[44]

[45] L. Mörl, D. Hoffmann, K. Matzen, C. Bornholdt G. G. Mekonnen, F. Reier, "Traveling Wave Electrodes for 50GHz Operation of Opto-Electronic Devices Based on InP", *Proceedings of IPRM 1999, Davos, Switzerland.* WeA1-3, pp 385-388, 1999.

[46] S. Akiyama, S. Hirose, T. Watanabe, M. Ueda, S. Sekiguchi, N. Morii, T. Yamamoto, A. Kuramata and H. Soda, "Novel InP-based mach-zehnder modulator for 40 Gb/s integrated lightwave source", *IEEE 18th International Semiconductor Laser Conference 2002*. TuC1, pp 57-58, 2002.

[47] UCSB standing H.-F. Chou, Y.-J. Chiu, J. E. Bowers, "Standing-Wave Enhanced Electroabsorption Modulator for 40Gha Optical Pulse Generation", *IEEE Photonics Tech. Lett.*, vol 15, no. 2, pp 215-217, Feb. 2003.

[48] UCSB absorption: Y.-J. Chiu, V. Kaman, S. Z. Zhang, and J. E. Bowers, "Distributed Effects Model for Cascaded Traveling-Wave Electroabsorption Modulator", *IEEE Photonics Tech. Lett*, vol. 13, no. 8, pp. 791-793, august 2001.

[49] NTT absorption: H. Takeuchi, "Ultra-fast electroabsorption modulator integrated DFB lasers", *Procedings of IPRM 2001*, pp. 428-431.

[50] hole pile-up:

[51] M. Suzuki, H. Tanaka, S. Akiba, "High-speed characteristics at high input optical power of GaInAsP electroabsorption modulators", *Electron. Letters*, vol. 24, no. 20, pp. 1272-1273, Sep. 1988.

[52] M. Suzuki, H. Tanaka, S. Akiba, "Effect of hole pile-up at heterointerface on modulation voltage in GaInAsP electroabsorption modulators", *Electron. Letters*, vol. 25, no. 2, pp. 88-89, Jan. 1989.

[53] D. Meglio, P. Lugli, R. Sabella, and O. Sahlén, "Analysis and optimization of InGaAsP electro-absorption modulators", *IEEE J. Quantum Electron.*, vol. 31, no. 2 , pp. 261-268, Feb 1995

[54] J. N. Hollenhorst, "Fundamental Limints on Optical Pulse Detection and Digital Communication", *IEEE J. Lightwave Technol.*, vol. 13, no. 6, pp. 1135-1145, 1995.

[55] Personick

[56] J. Bowers, C. Burrus, "Ultrawide-Band Long Wavelength p-i-n Photodetectors", *J. Lightwave technol.*, vol. LT-5, no. 10, pp 1339-1350, Oct. 1987.

[57] K. Kato, "Ultrawide-Band/High-Frequency Photodetectors", *IEEE Trans. Microwave Theory Tech.*, vol. 47, no. 7, pp 1265-1281, Jul. 1999.

[58] G. Jacobsen, J.X. Kan, I. Garrett, "Tuned Front-End Design for Heterodyne Optical Receivers", *J. Lightwave Technol.*, vol. 7, no. 1, pp 105–114, Jan. 1989.

[59] J. L. Hullet, T. V. Muoi, "A Modified Receiver for Digital Optical Fiber Transmission Systems", *IEEE Trans. Com.*, vol. COM-23, pp 1518-1521, Dec. 1975.

[60] M. S. Park, R. A. Minasian, "Ultra-Low_Noise and Wideband-Tuned Optical Receiver Synthesis and Design", *J. Lightwave technol.*, vol. 12, no. 2, pp 254-259, Feb. 1994.

[61] J. Bellon and M.J.N. Sibely, "Frequency response of transit time limited pin photodiode", *Electronics Lett.*, vol. 36, no. 14, pp. 1222-1223, July 2000.

[62] G. Lucovsky, R. F. Schwarz, R. B. Emmons, "Transit-Time Considerations in p-i-n Diodes", *J. Appl. Phys.*, vol. 35, no 3, pp. 622-628, Mar. 1964.

[63] For example: J. G. Proakis, M. Salehi, "Communication System engineering", Englewood cliffs, New Jersey: Prentice-Hall, chapter 7.2 and 11.2.3, 1994.

[64] R. J. Nuyts, L. D. Tzeng, O. Mizuhara and P. Gallion, "Effect of Transmitter Speed and Receiver Bandwidth on Eye Margin Performance of a 10Gb/s Optical Fiber Transmission System", *IEEE Photonics Tech. Lett.*, vol 9, no. 4, pp 532-534, Apr. 1997.

[65] For example: G. P. Agrawal, "Fiber-Optic Communication Systems", New York: Wiley, chapter 4.5, 1997.

[66] H.-J. Eul, B. Shiek, "A Generelized Theory and New Calibration Procedures for Network Analyzer Self-Calibration", *IEEE Trans. Microwave Theory Tech.* vol. 39, no. 4, pp 724- 731, April 1991.

[67] D. M. Pozar, *Microwave Engineering*, Reading, MA: Addison-Wesley, 1990, pp. 231-235.

[68]

Background on segmented Optical modulators

By Robert Lewén & Urban Eriksson 2003-03-20.

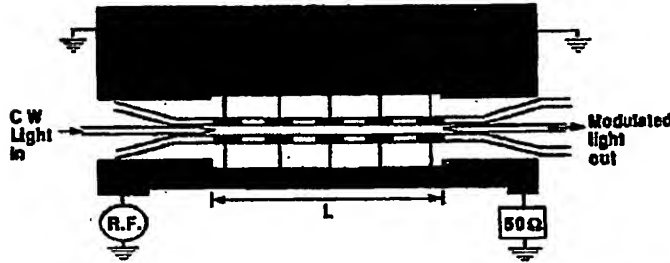## *The Original configuration by Walker [1]*

Fig. 1. Schematic of traveling-wave Mach–Zehnder modulator using capacitively loaded coplanar strip-line and three-guide coupler split/recombine regions.
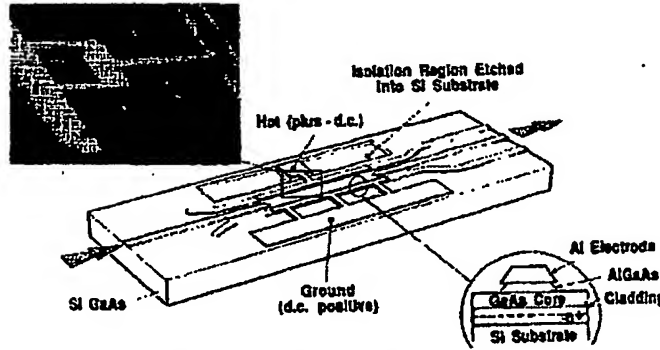
Fig. 2. GaAs–AlGaAs Mach–Zehnder modulator representative of technology used throughout this work. Lumped, single-sided drive is illustrated. Insets show the waveguide cross section and an SEM micrograph of the air bridge.

Figure 1 The original Walker implementation [1].

The original configuration [1] (Figure 1) consists of one passive microwave transmission line (TML) with characteristic impedance and propagation index

$$Z_p = \sqrt{\frac{L_p}{C_p}} \text{ and } n_p = c_0\sqrt{L_p C_p},\tag{1}$$

where L_p and C_p is the inductance and capacitance per unit length of the TML, respectively. The passive waveguide is capacitively loaded by a number of modulator sections each with a length l_m, a (center to center) spacing l_s, and a capacitance per unit length C_m. The resulting effective (Bloch) impedance and propagation index is then expressed as:

$$Z_B = \sqrt{\frac{L_p}{C_p + C_m\dfrac{l_m}{l_s}}} \text{ and } n_B = c_0\sqrt{L_p\left(C_p + C_m\frac{l_m}{l_s}\right)}\tag{2}$$

The optical and electrical velocity is matched ($n_B = n_o$) if [1]

$$C_m \frac{l_m}{l_s} = \frac{n_o^2 - n_p^2}{c_0^2 L_p} = \frac{n_o^2 - n_p^2}{c_0 Z_p n_p} \cdot \qquad (3)$$

Resulting in a characteristic impedance

$$Z_B = Z_p \frac{n_p}{n_B} = Z_p \frac{\sqrt{\varepsilon_{eff}}}{n_B} \qquad (4)$$

An alternative expression for (3) is then given as:

$$C_m \frac{l_m}{l_s} = \frac{n_B^2 - n_p^2}{c_0^2 L_p} = \frac{n_B^2 - n_p^2}{c_0 Z_B n_B} \qquad (5)$$

Example 1 (corresponding to [1]):
passive TML implementation as a co-planar strip on SI-InP (see [1] for GaAs)
ε_r=12.4, ε_{eff}=6.7.
With Z_B=50Ω, then Z_p=65Ω and $C_m * l_m/l_s$=95pF/m.
A typical C_m for an electroabsorption modulator (EAM) is at least 700pF/m, hence, l_m/l_s<0.137.

Example 2 (more similar to [2]):
TML implementation as a microstrip on BCB
ε_r=2.7, ε_{eff}≈2.
With Z_B=50Ω, then Z_p=119Ω and $C_m * l_m/l_s$=187pF/m.
Using a typical EAM C_m of minimum 700pF/m, results in l_m/l_s<0.27.

The disadvantage with these implementations will be discussed in the suggested improvements in the following sections.

The original Walker configuration [1] is, to my knowledge, not protected by any patents.
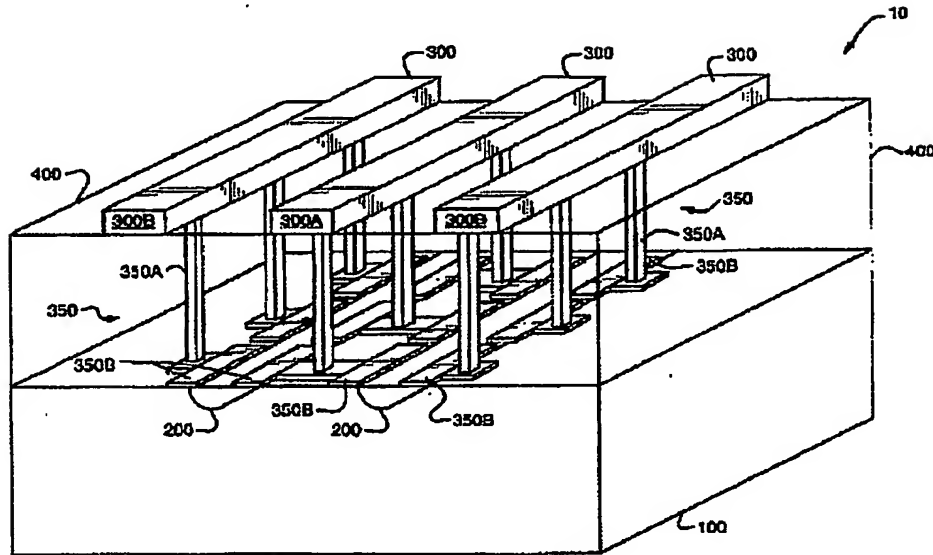
The modified Betts approach [2]

Figure 2. Modified version by Betts [2]. ε_{eff} is reduced by an additional thick layer with low εr, the modulator sections is contacted to the passive TLM with vertical vias, or "conductive legs". (The original Walker implementation uses horizontal arms instead (Figure 1)).

A disadvantage with the Walker implementation according to example 1 in section 1 is the low duty cycle (l_m/l_s) between active and passive optical waveguide (WG) sections. This is particularly a problem for an EAM due to a typically high C_m. Betts [2] have therefore proposed that the passive electrode should be implemented with an additional substrate layer with low dielectric (claim 2) (Figure 2), for example polyamide or air (claim 3, claim 6). This implementation decreases ε_{eff} (claim 5). The modulator sections can be connected with vertical vias, or conductive legs (claim 4).

And the list goes on with 27 claims in total, all referring to electro-optic (EO) modulators. There are no claims concerning electroabsorption modulators, or optical modulators in general.

The important improvement in [2] is the introduction of an additional dielectric layer that reduces ε_{eff}. This improvement leads to a lower duty cycle (l_m/l_s) and a reduced total device length for a given effective modulator length. See example 2 in section 1.
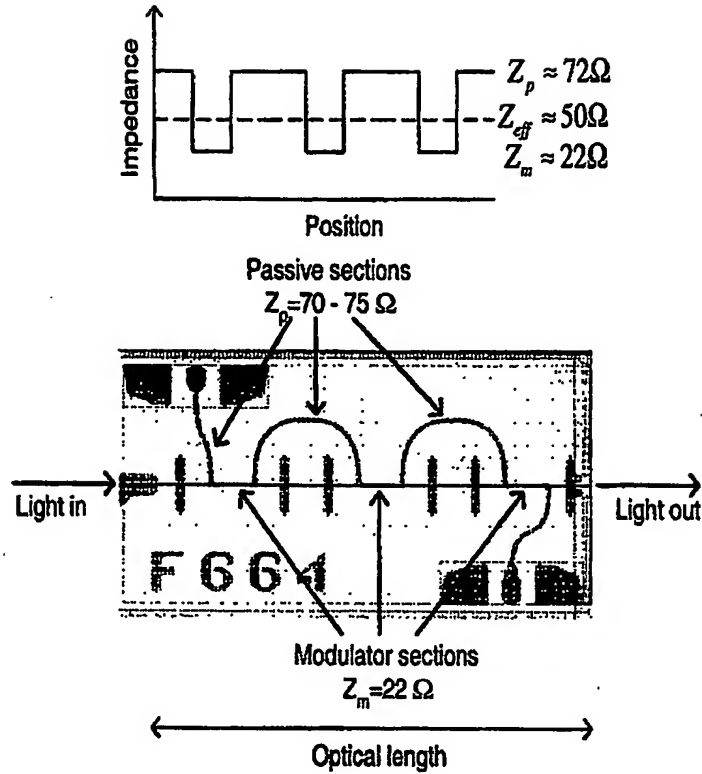
Our approach

Figure 3. Our implementation with a different length of the TML (l_{TML}), compared to the optical WG ($l_{optical}$).

In our implementation we have implemented the passive WG as a microstrip on BCB (example 2 in section 1). The low value of $\varepsilon_{eff}\approx 2$ indicates that the passive WG should be designed with a characteristic impedance of $Z_p=119\Omega$. This high impedance level is however not practical. For example: a plated microstrip with a width of 6μm and a plated height of 3μm with a 7μm thick BCB layer has (experimentally) resulted in an impedance of $Z_p=75\Omega$. It is therefore not possible to reach 50Ω and velocity matching with this implementation according to the design rules proposed by Walker [1].
The solution to this problem is to delay the electrical wave by making the TML longer than the corresponding optical waveguide (Figure 3 implemented as Figure 2). This modifies (4,5) to:

$$Z_B = Z_p \frac{n_p}{n_B} \frac{l_{TML}}{l_{optical}} = Z_p \frac{\sqrt{\varepsilon_{eff}}}{n_B} \frac{l_{TML}}{l_{optical}} \tag{6}$$

$$C_m \frac{l_m}{l_s} = \frac{n_B^2 - \left(n_p \frac{l_{TML}}{l_{optical}} \right)}{c_0 Z_B n_B} = C_{eff} \tag{7}$$

Z_p can now be chosen arbitrarily (larger than the required Z_B) and the velocity matching is adjusted by the length ratio. There is however a penalty as a lower Z_p results in a lower duty cycle between active and passive optical waveguide (l_m/l_s). Z_p

should be maximized with respect to the resulting electrical loss in the structure, as this is ultimately the limitation for the device bandwidth.

Example 3:
TML implementation as a microstrip on BCB with a maximum Z_p of 75Ω, using a capacitively loaded line.
$\varepsilon_r=2.7$, $\varepsilon_{eff}\approx2$.
With $Z_{tot}=50Ω$, then $l_{TLM}/l_{optical}=1.6$ and $C_m*l_m/l_s=130pF/m$.
Using a typical EAM C_m of minimum 700pF/m, results in $l_m/l_s<0.185$.

The design can be further improved by reducing the feed-lines [1] (Figure 1) or conductive legs [2] to a minimum. Ideally the modulator should be an integrated part of the passive WG, i.e., a cascaded structure (Figure 3) [4]. This results in:

$$\left(C_m - C_p\right)\frac{l_m}{l_s} \approx \frac{n_o^2 - \left(n_p \frac{l_{TML}}{l_{optical}}\right)^2}{c_0 Z_B n_o} = C_{eff} \tag{8}$$

There are two reasons for this:

1) The duty-cycle is improved by a ratio of

$$ratio \approx \frac{C_m}{C_m - C_p}, \tag{9}$$

or typically 10% for an EAM implementation ($C_m\approx700$ pF/m, $C_p\approx70$ pF/m).

2) We avoid the implementation with conductive legs, which could make the design similar to [2].

The additional Walker patent [3]

This patent suggests a modification of the original implementation [1]. An additional capacitance (34 in Figure 4) is introduced in order to modify the modulation strength of one arm in a MZI. This creates an unbalance in the MZI, which can be utilized for chirp control.
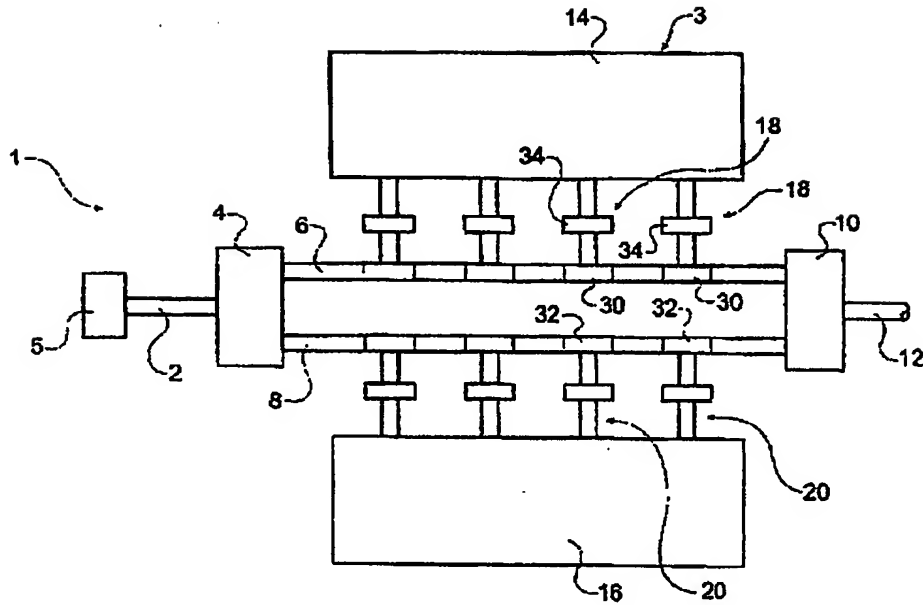
Figure 4. The additional Walker patent [3]

References

[1] R. G. Walker, "High-Speed Semiconductor Intensity Modulators", *IEEE J. of Quantum Electron.*, vol. 27, no. 3, pp 654-667, 1991.

[2] G. E. Betts (MIT), "Velocity Matching Electrode Structure for Electro-Optic Modulators", US Patent 6,310,700.

[3] R. G. Walker, E. M. Kimber (NORTEL), "Optical Modulator", WO Patent 02/50606 A1.

[4] S. Akiyama, S. Hirose, T. Watanabe, M. Ueda, S. Sekiguchi, N. Morii, T, Yamamoto, A. Kuramata and H. Soda, "Novel InP-based mach-zehnder modulator for 40 Gb/s integrated lightwave source", *IEEE 18th International Semiconductor Laser Conference 2002.* TuC1, pp 57-58, 2002.

CLAIMS

1. An optical modulator, divided into at least two active segments separated by at least one passive segment, the modulator comprising

   an optical waveguide with an optical group index (n_o), having an optical signal propagating at an optical velocity (v_o), and

   a microwave transmission line with an electrical propagation index (n_p), having an electrical signal propagating at an electrical velocity (v_e),

   wherein the electrical propagation index (n_p) of the unloaded microwave transmission line is lower than the optical group index (n_o) of the optical waveguide,

   characterized in that

   the loading and length of the microwave transmission line are adjusted for a specific Bloch impedance and electrical velocity (v_e).

2. An optical modulator according to claim 1, **characterized in that** the electrical velocity (v_e) in the adjusted microwave transmission line is substantially equal to the optical velocity (v_o) in the optical waveguide.

3. An optical modulator according to any of claims 1 or 2, **characterized in that** the length of the microwave transmission line from the center of one active segment to the center of the adjacent active segment is longer than the length of the corresponding optical waveguide from the center of one active segment to the center of the adjacent active segment.

4. An optical modulator according to any of claims 1 - 3, **characterized in that** the active segment of the optical modulator is a microwave transmission line and is cascaded in series with the microwave transmission line of the passive segment.

5. An optical modulator according to any of claims 1 – 4, **characterized in that** the optical modulator is an electro-

absorption modulator.

6. A method for adapting the impedance in an optical modulator which is divided into at least two active segments separated by at least one passive segment, wherein the modulator comprises

an optical waveguide with an optical group index (n_o), having an optical signal propagating at an optical velocity (v_o), and

a microwave transmission line with an electrical propagation index (n_p), having an electrical signal propagating at an electrical velocity (v_e),

wherein the electrical propagation index (n_p) of the unloaded microwave transmission line is lower than the optical group index (n_o) of the optical waveguide, **characterized by**

adjusting the loading and length of the microwave transmission line for a specific Bloch impedance and electrical velocity (v_e).

7. A method according to claim 6, **characterized by** adjusting the loading and length of the microwave transmission line in such a way that the electrical velocity (v_e) in the adjusted microwave transmission line becomes substantially equal to the optical velocity (v_o) in the optical waveguide.

8. A method according to any of claims 6 or 7, **characterized by** adjusting the length of the microwave transmission line in such a way that the length from the center of one active segment to the center of the adjacent active segment becomes longer than the length of the corresponding optical waveguide from the center of one active segment to the center of the adjacent active segment.

9. A method according to any of claims 6 - 8, **characterized by** implementing the active segment of the optical

modulator as a microwave transmission line and cascading it in series with the microwave transmission line of the passive segment.

10. A method according to any of claims 6 – 9, **characterized by** the optical modulator being an electro-absorption modulator.